SIMULATION-LED DESIGN FOR OPTIMIZATION OF INNOVATIVE ACOUSTIC PHANTOM AND THE ICE CATHETER CALIBRATION METHOD

E. Adawi M.Sc., R. Peled Ph.D.
Research and Development System Engineering Department, Biosense Webster (Israel) Ltd., Yokneam, Israel

Introduction

Intracardiac Echocardiography (ICE) ultrasound imaging of cardiac cavities is a known diagnostic and monitoring technique, used during interventional cardiology and electrophysiology (EP) procedures.

The SOUNDSTAR® ICE Catheter, manufactured by Biosense Webster, Inc., enables locating the position and registration between ultrasound images and magnetic maps of cardiac cavities. It comprises both an acoustic imaging device (a one-dimensional phased array), and an electromagnetic (EM) tracking sensor, each with its own coordinate system. To correlate locations measured using both sensors, a registration (calibration) procedure is required to produce reliable images and anatomical structure locations.

Most ultrasound calibration techniques known today are intended for external probes, and are not adapted to the characteristics of catheters. The required high-level operator skills and time-consuming procedures are the main disadvantages of such techniques.

Acoustic simulations, created with COMSOL Multiphysics® modeling software, were performed to optimize innovative phantom design and calibration method, by adapting them to catheter characteristics.

Theory Background

The clinical requirement for target localization accuracy between magnetic cardiac maps and ultrasound cardiac maps, generated by an ICE catheter, is typically under 5mm [4]. In particular, SOUNDSTAR® Catheter calibration procedure accuracy is intended to withstand much stricter and challenging requirements in laboratory conditions.

The main objective of the research documented herein was to improve and simplify the calibration method of the SOUNDSTAR® Catheter. It does not focus on a comprehensive simulation of the acoustic transducer performance, pulse transmission, beam formation, echo reception, or signal processing for ultrasound image reconstruction. The research does, however, focus on optimizing the design and characteristics of a dedicated acoustic phantom and to adapt it to the characteristics of ICE catheters.

The reflection of ultrasound waves is generally categorized as either specular or diffuse echoes. Specular echoes originate in relatively large objects that are regularly shaped and have smooth surfaces, where the sound wave is reflected in a singular direction. Specular reflectors are mostly apparent when the sound wave is perpendicular to the target. Scattered echoes originate in smaller objects that are less reflective and irregularly shaped, causing a uniform manner of reflection in various directions, relative to the transmitted beam. This reflection is less angle-dependent and less echo-intense. When the ultrasound wavelength (λ) is much greater than the structure it comes in contact with, a Rayleigh scattering occurs due to wave interference, causing a reflection with uniform amplitude in all directions and a small echo returning to the transducer (i.e., red blood cells).

Backscatter is the reflection of waves, toward the transducer. It is a diffuse reflection due to scattering, as opposed to specular reflection, as is from a mirror (i.e., the same principle as in a RADAR system).

This simulation studies were designed for understanding the performance and the acoustic characteristics of multiple tested acoustic reflectors (targets). The goal is to develop an ideal acoustic diffuse reflector for calibration purposes, by improving its visualization in ultrasound, which facilitates the automatic identification of target using image processing techniques and enables automatic calibration. An optimal calibration target will generate sufficient detectable backscatter, independent of the acoustic wave angle of incidence. Such a target will reduce dependency on operators and also minimize mechanical alignment challenges

(between the ultrasound transducer and the acoustic target).

COMSOL Simulations

Finite Element Method (FEM) is a powerful and comprehensive tool for this application. Additionally, it is necessary to have a deep insight of the physics of the simulated problem to develop a sufficient model.

The linear, one-dimensional phased-array transducer of the SOUNDSTAR® Catheter (**Figure** 1), which is operated to create a two-dimensional image (also known as fan) in the plane of the ultrasonic scan beam (referred to herein as the "beam plane" or "in-plane".

Figure 1. SOUNDSTAR® Catheter and its tip

In the present work, numerically efficient, easy-to-implement, and relatively simple 2D FEM models were developed, using COMSOL Multiphysics® 5.2, to understand the wave propagation and acoustic field behavior. This is a result of incident plane wave reflection by various target designs. The models were developed assuming that the target is located in the focal zone of the sound beam, and without taking into consideration the out-of-plane dimension.

Both transient and frequency domain interfaces of the COMSOL® Pressure-Acoustic module were used to analyze pressure field variation for propagation of acoustic plane waves in the medium, and their reflections from an acoustic target back into the transmission transducer (backscatter). The transient interface is used to solve the scalar wave equation in the time domain, while the frequency domain interface is used to solve the Helmholtz equation in the frequency domain for given frequencies.

As is well known in the FEM field, computational acoustics is challenging, especially in the space and time domains, due to meshing considerations, time stepping, modeling open boundaries, etc. The recommended mesh size for resolving wave equations in space is $h \leq \lambda/5$, while the recommended time stepping for resolving waves equations in time is $\Delta t \leq \frac{T}{25}$, where T is the cycle length time (according to the Courant–Friedrichs–Lewy condition).

The constrains above cause the time domain analysis to grow to extremely large calculation (excessively) time, in addition to the need for high computational power. Therefore, the usage of the transient interface solution was limited to a small dimensions model, representing the tested target vicinity, simulating the near-field reflection of single sinusoidal pulse in an amplitude of 1[Pa], transmitted perpendicular (relative to the target). The absolute value of the pressure is not of interest, where the relative pressure differences that occur are those of interest. Those models were used for initial understanding of the acoustic waves scattering in the medium for various target shapes.

Conversely, fast and simple models have been developed for steady-state analysis, using the frequency domain interface to solve the problem of the scattered acoustic field both in the near and far fields. Those models covered numerous tested parameters, including target shape, size, incident wave angle, and distance from the transducer.

Typical operation frequencies of medical diagnostic ultrasound devices range between 2–18 MHz, where the higher frequencies have a correspondingly smaller wavelength, and provide better resolution. They can also be used for discernment of smaller details.

The ultrasound wave is mainly determined by its wavelength, frequency, velocity, and intensity. Velocity of ultrasound, 1540 [m/s] in the soft tissues, depends on the medium temperature. Since the calibration is performed in ambient room conditions (assumedly $25°C$), the speed of the sound was determined according to material properties from the COMSOL library. Representing a reasonable wave frequency of 5 MHz was selected (equivalent to $\lambda = 0.3mm$), taking into consideration the typical operation range and the simulation computation and performance constrains.

Figure 2 describes the ambient geometry used in the analysis. A finite 2D rectangle of 20 x 13mm was used to represent the region of interest of a virtually unbounded water tank. For the frequency domain analysis, a Perfectly-Matched-Layer (PML) was added to the ambient rectangle. A 10mm linear line was used at the left boundary to represent the transducer area for calculating the backscatter energy.

Four typical target intersection shapes were examined (see **Figure** 3): planar plate (A), arrow (B), corner reflector (C), and circle (D). The targets were simulated as to be made of a hard-acoustic material (perfect reflector) and positioned 10mm

perpendicularly in front of the central line of the transducer. Shape comparison was performed for relatively large target sizes in relation to the wavelength, (target size of $10\lambda = 3mm$).

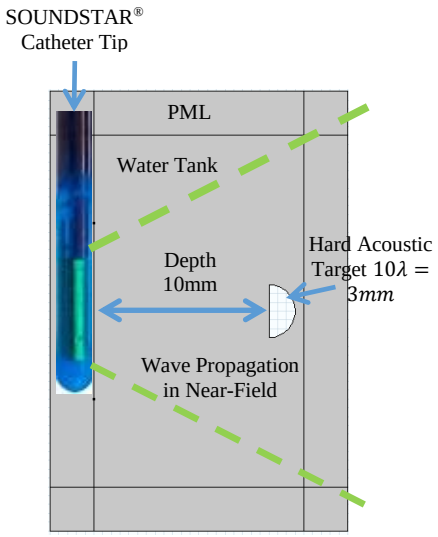

Figure 2. 2D model geometry for planar target

The Plane Wave Radiation boundary condition was used for wave propagation in the transient model to simulate an unbounded model. This condition allows an outgoing plane wave to leave the modeling domain with minimal reflections (assuming that the angle of incidence is near normal). Incident Pressure Field boundary condition was used to apply an incoming plane wave. A single sinusoidal pressure pulse was transmitted, in an amplitude of 1Pa, which proceed in the horizontal axis of the FEM.

The Background Pressure Field node was used in the frequency domain model for simulating an incident of a continuous plane pressure wave, in order to study the scattered pressure field – which is defined as the difference between the total acoustic pressure field and the background pressure field. The initial pressure condition was set to zero. PML was used to simulate wave propagation of an unbounded model, as a virtual infinite domain surrounding the physical region of interest. PML is supposed to absorb all outgoing wave energy. The Sound Hard Boundary condition was applied to the external boundary of the PML.

The Far-Field Calculation node was used on the internal boundaries of the PML, to perform the transformation from the near-to-far-field for a specific acoustic variable. This enables calculating the pressure field outside the computational domain (including far-field backscatter), without the need of enlarging the domain dimensions. It was used to minimize the physical dimensions of the model. RADAR cross-section (RCS) and exterior far-field calculations were made at a distance of $8.33cm$, corresponding with the simulated problem and the selected wavelength and transducer dimension of $10mm$.

Three different angles of incidence were simulated by the Parametric Sweep feature, to study its effect on the backscatter: 0° (perpendicular to target), 15°, and 30° (angles are relative to the model horizontal axis).

Methods

Target comparisons were made, relative to various parameters, such as geometrical shape, size, distance from the transducer, spatial distribution, and intersection with the ultrasound fan. The study included analysis of wave propagation and interference in the near and far fields by means of reflectivity (or echo strength), RCS, and reflection directivity (with dependency on incident wave orientation).

By employing RCS analysis, in this study we will try to solve the far-field problem in a similar way as the RADAR problem approach. An object reflects a limited amount of the transmitted energy back to the source. The reflected energy is mainly influenced by target shape, material, size (in relation to the wavelength), and the incident and reflection angles. RCS is a measure of a target's ability to reflect signals in the direction of the receiver, and indicates how detectable an object is by RADAR. A larger RCS indicates that an object is more easily detected. It is mainly a property of the target's reflectivity, and not affected by the transmitter properties or distance to target.

Simulation Results

Figure 3 shows the total acoustic pressure field simulation results in the time domain for all tested targets. The images were captured shortly after the incident wave struck the target. Image A represents the planar target, shows that the reflected wave has high amplitude, is focused (to a similar beam width as that of the target), and travels in a singular direction (as opposed to the incident wave). Image B represents the arrow target and shows that such a target, in fact, dissipates the wave sideways, causing the echo received in the transducer to be negligible. Image C represents the corner-reflector target and shows that the reflected wave has a strengthened

amplitude, is focused (more than that of Image A), and travels in a singular direction (as opposed to the incident wave). There are also some interferences from the sharp edges. This target reflects waves back directly toward the source.

Image D represents the circle target and shows that the reflected wave expands circularly, has a moderate amplitude, and uniform manner — resembling a typical diffuse reflector.

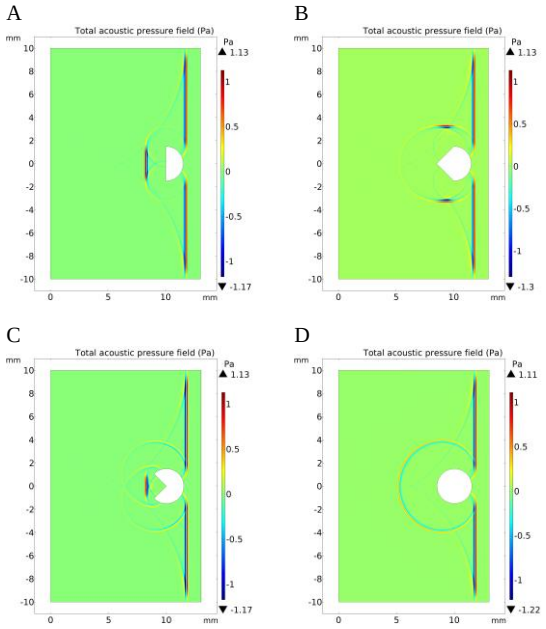

Figure 3. Total acoustic pressure field reflection in the time domain for all tested targets

The echoes received from each tested target, calculated as an average of total acoustic pressure along the transducer line, are consistent with the behaviors described in **Figure** 3.

Figure 4 shows the RCS simulation results in the frequency domain for all tested targets as a function of 3 incident angles and is calculated for the absolute scattered pressure field. Image A represents the planar target and shows that the reflected wave has high amplitude (is not affected by the incident angle), is focused, travels in a singular direction, a mirror of the incident angle — typical specular reflection. The backscatter ranges from 60% at a 0° angle to 0.5% at a 30° angle. Therefore, the visibility of this target is limited by its transmitting angles. Image B represents the arrow target and shows that the incident wave dissipates sideways, such that there is a dip at the angle of incident and most of the field that hits the target reflects to the sides. The backscatter ranges from 2% at a 0° angle to 3.3% at a 30° angle (i.e., the echo received in the transducer is negligible and resembling behavior in stealth aircraft, vis-à-vis RADAR). The visibility of such a target in ultrasound is mainly due to the reflections that are received from the straight surfaces, when they fall within the field of view. Consequently, this target does not fit optimization of calibration purposes.

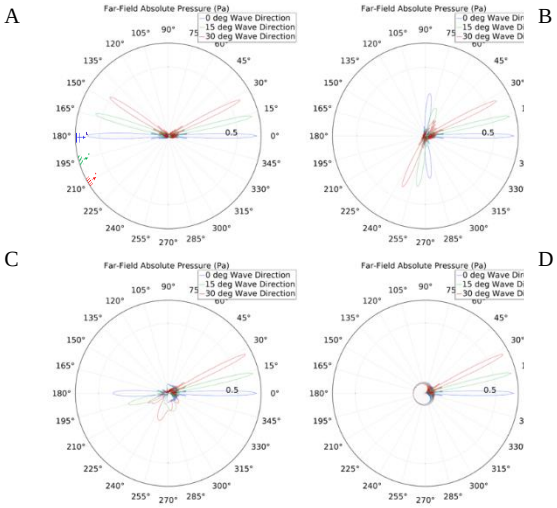

Figure 4. RCS of far-field absolute scattered pressure for all tested targets as function of 3 incident angles

Image C represents the corner-reflector target and shows that the reflected wave is focused, and travels in a singular direction, as opposed to the incident wave, up to a certain angle (with a limited range). The reflection amplitude decreases, as the incident angle increases. The backscatter ranges from 40% at a 0° angle to 12% at a 30° angle, while the peak reflection (at 30°) is sideways.

Image D represents the circle target, shows that the reflected wave demonstrates a moderate and uniform manner reflection of about 10% backscatter, and expands circularly (resembling a typical diffuse reflector, as in the time-domain behavior).

This target reflection is independent of the incident angle. These results represent the wave propagation and scattered pressure, as a result of single incident wave direction. A phased-array transducer scans the imaged plane by many waves transmitted in different directions. Typically, ICE image is acquired at 90° (±45°) opening angle. Therefore, the total echo strength is affected by all backscatters from all transmitted wave directions. Thus, if the target shape guarantees diffuse reflection, a small backscatter will be received, independent of the incident angle. However, the total echo of a circular target is much greater (rounded surfaces always have some point of the surface normal to the wave source).

As in **Figure** 4, **Figure** 5 shows the RCS, which corresponds with a very small circle target (1λ diameter). Different circle target sizes (ranging between 1-20λ) were examined. The results showed a similarity to that described in **Figure** 4 D. In addition, as the target size increases, so does its scattered pressure intensity (approximately proportional to the root-square of the relative size). When the target size reached the relative size of λ, an interesting interference pattern occurs. Despite that, the peak reflection is still in the direction of the transmitter, side loops were observed. In this case, the target continues to reflect in various directions, but in a narrower range.

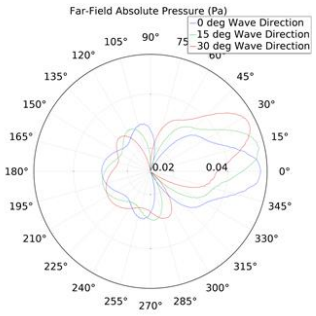

Figure 5. RCS of far-field absolute scattered pressure for small circle target (1λ diameter) as function of 3 incident angles.

Experimental Results

A few validation prototypes with different parameters were produced that were based on the simulation results, and through which the conclusions were proven.

Various target shapes, sizes, and geometrical designs were examined. The best performances were obtained by a small and rough arch-shaped target (see the left of **Figure** 6), where the catheter is positioned in the arch center, so that in each orientation, the ultrasound fan intersects it in a similar ultrasonic view. On the right, the corresponding ultrasound image of $1mm$ target thickness is displayed.

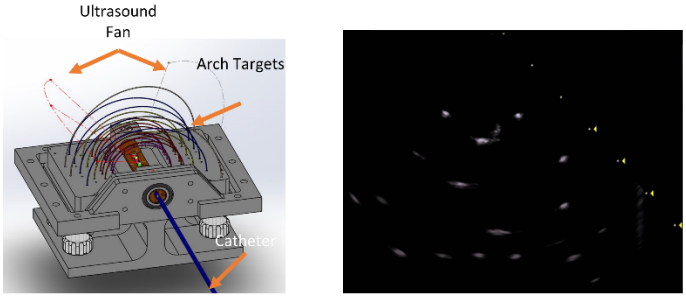

Figure 6. (Left) Arches acoustic phantom, (right) its ultrasound image.

Test results showed that a total calibration error of less than $0.3mm$ in the in-plane can be achieved, using precise arch targets of $1mm$ thickness. The calibration accuracy was measured as the root-mean-square error for target localization between ultrasound images and reference mechanical positions. Calibration accuracy is mainly affected by target thickness, its manufacturing accuracy, the total number of targets, and their spatial dispersion.

Discussion

Figure 3 and **Figure 4** show that a target that is made from planar surfaces, are strong specular reflectors, and are not suitable for calibration purposes. Also, an arrow-shaped target is not suitable for the purpose of the study, due to visibility issues. Despite the fact that a corner-reflector target guarantees good backscatter in a singular direction, the reflection amplitude is not uniform, and reflection is guaranteed only up to a certain angle because it has a limited visibility range. As is well known, such a target is visible when it is placed inside the beam scanning range and angled toward the transducer. Accordingly, the transducer-target mechanical alignment is critical. This adds to the complexity of production (especially when it comes to very small physical dimensions). Therefore, these options are less desirable.

In contrast, a circle-shaped target reflects waves in a wide range of directions and a circularly uniform expanding manner, making this target reflection similar to a diffuse reflector. This target reflection is independent of the incident angle, making transducer-target mechanical alignment easier. The described behavior derives mainly from the rounded geometrical shape, and the wide beam width, relative to the target size. Rounded surfaces always have some point of the surface normal to the wave source, which ensures that some portion of the energy will return to the transmitter, regardless of the source-

target alignment. The round-shaped target demonstrated the most stable, consistent, and better performance for the intended purpose from all tested targets, including the ease of manufacturing and accurate automatic detection, and minimal alignment, making it a preferred choice.

Although smaller target sizes mean lower echo (according to **Figure** 5), better image resolution is acquired (as assessed by point-spread function in experimental results, and also according to literature). Trade-offs have appeared between target size, scatter directivity, and image resolution. Large targets ($> 10\lambda$) provide higher echo, and demonstrate less orientation dependency than small targets (in the order of λ). On the other hand, the smaller the target; the better the image resolution and the better the automatic identification (in terms of accuracy and simplicity).

Experiment results also showed that surface irregularities (roughness) in the order of sub λ, make the reflection better and diffusive (in accordance with related literature).

The phantom design is subject to many physical constrains and manufacturing considerations. The more targets used; the better the total calibration accuracy. Thus, a smaller target is a possible advantage for dealing with space constrains, in addition to achieving better image quality (small and uniform spots, as in **Figure** 6). However, a desired very thin, rough, and arch-shaped target is subject to many manufacturing, and reliability challenges. Thus, the above trade-off must be considered.

Conclusions

An optimal target for ICE catheter calibration was found to be minimal (smaller than the beam-width) and yet larger than λ (to avoid interferences), with a rounded rough surface (that is sub λ for diffuse reflection), made of a hard-acoustic material, and perpendicular to the ultrasound fan. The arch target with these properties is designed to appear as a dot in an ultrasound image that enables automatic and accurate target identification, simplifying the calibration, and reducing user dependency. The research led to the development of an innovative calibration technique that yields significant improvements in ICE catheter calibration, and a new patent application.

Some future researches are still required, which will focus on better characterization and simulation of the specific ultrasound device, such as the wave-front propagation profile at different distances (plane, cylindrical, spherical, etc.)

References

1. E. Adawi et al., “Simulation-Led Design to Optimize Innovative Acoustic Phantom Design and Calibration Method, for Intracardiac Ultrasound Localization Catheter”. U.S. Provisional Application No. 62/684942 (June 2018).
2. R. Peled, E. Adawi et al., "Acoustic Phantom and Method for Intracardiac Ultrasound Localization Catheter". U.S. Patent BIO5930USNP (September 2018).
3. Haim Azhari, “Ultrasound Physical Principles and Medical Applications”. Technion - Israel Institute of Technology, Israel (2006).
4. C. A. Linte, et al. "Calibration and Evaluation of a Magnetically Tracked ICE Probe for Guidance of Left Atrial Ablation Therapy." Proceedings of SPIE - the International Society for Optical Engineering, 8316 (2012).
5. COMSOL Multiphysics® Acoustic Module User Guide

Acknowledgements

I want to express great appreciation to my colleague, Mr. Moshe Chertoff, a Senior Technical Communicator, for editing this paper.